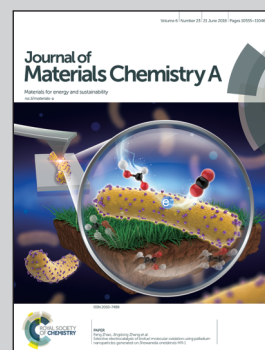


**Showcasing a study of the high-efficient decolorization of methylene blue using FePC amorphous alloy by the group of Prof. Baolong Shen at Southeast University, China.**

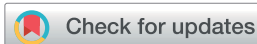
Investigation of FePC amorphous alloys with self-renewing behaviour for highly efficient decolorization of methylene blue

The high degradation efficiency of FePC amorphous alloys results from the fast mass and electron transport due to the formed 3D nanoporous structures during reaction, as well as the galvanic cells formed between the strong Fe-C and the weak Fe-P bonds. The unique “self-renewing” behaviour of FePC amorphous ribbons during cyclic tests explains their extremely long service life.

**As featured in:**



See Chenglin Chu,  
Baolong Shen *et al.*,  
*J. Mater. Chem. A*, 2018, **6**, 10686.

Cite this: *J. Mater. Chem. A*, 2018, 6, 10686

## Investigation of FePC amorphous alloys with self-renewing behaviour for highly efficient decolorization of methylene blue

Qianqian Wang,<sup>ab</sup> Mingxiu Chen,<sup>ab</sup> Pinghua Lin,<sup>ab</sup> Zhiqiang Cui,<sup>ab</sup> Chenglin Chu<sup>\*ab</sup> and Baolong Shen<sup>†abc</sup>

FePC amorphous ribbons using Fenton-like reactions are proved to show excellent degradation performance in wastewater treatment for the first time by decolorizing methylene blue (MB). Compared to the widely investigated FeSiB amorphous ribbons for decolorization, FePC alloys have higher degradation efficiency and lower reaction activation energy, which comes from the fast mass and electron transport due to the 3D nanoporous structures formed during the reaction, as well as the galvanic cells formed between the strong Fe–C and the weak Fe–P bonds. The observed unique “self-renewing” behaviour of FePC ribbons during cyclic tests explains their extremely long service life. The FePC amorphous ribbons are applicable in acidic MB solutions, but not in neutral or alkaline solutions. The highest degradation efficiency is achieved when the initial pH = 3 and the initial H<sub>2</sub>O<sub>2</sub> concentration is 5 mM. The time required for the decomposition of MB drops with the increase of the ribbon dosage or the decrease of the initial MB concentration. This work not only provides a new highly efficient and low-cost solution for wastewater remediation, but also extends the application fields of FePC amorphous alloys.

Received 13th February 2018  
Accepted 23rd March 2018

DOI: 10.1039/c8ta01534a

rsc.li/materials-a

## Introduction

Synthetic dyes are widely used in the textile industry, causing serious environmental problems in wastewater disposal as they are not only cancerogenic and teratogenic, but also chemically stable and difficult to decompose.<sup>1–6</sup> Tremendous efforts have been made during the last several decades to reduce their deleterious impacts, including physical adsorption using activated carbon<sup>7</sup> and clays,<sup>8</sup> biological degradation using microorganisms,<sup>9</sup> as well as chemical degradation using advanced oxidation processes,<sup>10</sup> nanoscale bimetallic particles,<sup>11</sup> zero valent metals,<sup>12</sup> *etc.* However, the obvious drawbacks of these methods, such as low efficiency, high cost and/or short service life, continuously drive the exploration of advanced materials for the degradation of synthetic dyes in polluted water.<sup>13</sup>

Recently, amorphous alloys, including Fe-,<sup>14–24</sup> Mg-,<sup>25–30</sup> Al-,<sup>31,32</sup> and Co-<sup>33,34</sup> based amorphous thin ribbons, fine powders and nanoporous structures, have been proved to exhibit relatively satisfactory performance in wastewater remediation for removing synthetic dyes and other organic pollutants like

phenol and chemical oxygen demand (COD). Generally, the thermodynamically unstable state, the high residual stress and the large amount of unsaturated sites on the surface of amorphous alloys are believed to be the reasons for their excellent decolorization ability.

Among all the amorphous alloys investigated for dye degradation, Fe-based amorphous alloys have attracted the most attention due to their low material cost and high decomposition efficiency. Most of the Fe-based amorphous alloys investigated for decolorization are Fe–Si–B systems, or Fe–Si–B minorly alloyed with other elements, as Si and B form a non-compact layer on the surface of the alloys and benefit the electron transfer.<sup>35</sup> Wang *et al.* proved that ball-milled Fe<sub>73</sub>Nb<sub>3</sub>Si<sub>7</sub>B<sub>17</sub> powders exhibit much higher efficiency in degrading direct blue than their gas-atomized counterparts because of the larger specific surface area provided by the rough surface topography from ball-milling.<sup>15</sup> When decomposing methylene blue, ball-milled amorphous Fe<sub>78</sub>Si<sub>9</sub>B<sub>13</sub>/TiO<sub>2</sub> powder composites exhibited 60% and 40% higher degradation efficiency than pure TiO<sub>2</sub> powders, and crystalline Fe<sub>78</sub>Si<sub>9</sub>B<sub>13</sub> alloy/TiO<sub>2</sub> powder composites, respectively.<sup>36</sup> Kinetic analysis of the degradation process of acid orange II using amorphous and partially crystallized FeMoSiB ribbons revealed that the reaction rate was controlled by available reaction sites on the surface of the ribbons.<sup>37</sup> Minor addition of Y into FeSiB amorphous powder largely improved its dye degradation efficiency by introducing heterogeneous structures consisting of local Fe-rich and Fe-poor atomic

<sup>a</sup>School of Materials Science and Engineering, Southeast University, Nanjing 211189, China. E-mail: clchu@seu.edu.cn; blshen@seu.edu.cn; Tel: +86 15852943974

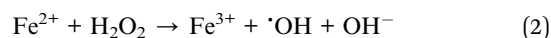
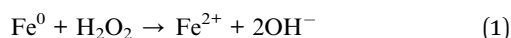
<sup>b</sup>Jiangsu Key Laboratory of Advanced Metallic Materials, Southeast University, Nanjing, 211189, China

<sup>†</sup>Institute of Massive Amorphous Metal Science, China University of Mining and Technology, Xuzhou 221116, China

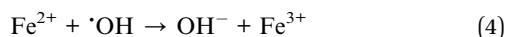
clusters that form galvanic cells within the alloy.<sup>19</sup> Extremely high degradation efficiency of orange II was achieved using FeSiBNbCuNi nanocrystalline ribbons due to the galvanic cells formed between multiple crystalline phases, which accelerate the rate of electron transfer.<sup>20</sup>

Other than the widely studied FeSiB system, the FePC amorphous system is another major category of amorphous alloys with distinct thermal and mechanical behaviour. Although the atomic sizes of P and C are similar to those of Si and B, the glass-forming ability of FePC amorphous alloys is larger than that of FeSiB amorphous alloys as Fe<sub>80</sub>P<sub>13</sub>C<sub>7</sub> is the only successfully synthesized ternary Fe-metalloid-based bulk glassy alloy,<sup>38</sup> which guarantees the FePC system more advantages in large-scale industrial applications. Since the first Fe<sub>80</sub>P<sub>13</sub>C<sub>7</sub> amorphous foil was prepared by Duwez in 1967,<sup>39</sup> the atomic, electronic, magnetic and mechanical properties, as well as the crystallization behaviour of the FePC amorphous system have been thoroughly studied.<sup>40–43</sup> A bulk Fe<sub>80</sub>P<sub>13</sub>C<sub>7</sub> glassy alloy with a diameter of 2.0 mm has been successfully synthesized *via* fluxing and J-quenching techniques,<sup>38</sup> presenting an extraordinary magnetocaloric effect and the largest refrigerant capacity among all the ternary Fe-based amorphous alloys.<sup>44</sup> However, no investigation has been made on the decolorization performance of FePC amorphous alloys.

Fenton/Fenton-like reactions are highly efficient advanced oxidation processes (AOPs) in wastewater remediation by producing reactive species with a high redox potential to decompose stable and harmful industrial organic effluents into nontoxic and ubiquitous substances.<sup>45,46</sup> The process of Fenton-like degradation of synthetic dyes with Fe-based amorphous alloys has been revealed to occur in three steps:



H<sub>2</sub>O<sub>2</sub> react with the zero-valent iron on the surface of the Fe-based amorphous alloy to produce Fe<sup>2+</sup>, which is the necessary catalyst for the following Fenton reaction. The as-produced highly reactive hydroxyl  $\cdot\text{OH}$  in eqn (2) is able to oxidize and decompose the organic pollutants from waste water, including synthetic dyes.<sup>18,47</sup> Besides, the Fe<sup>2+</sup> produced from eqn (1) is also oxidized by the hydroxyl to Fe<sup>3+</sup>, as shown in eqn (4):



In this paper, we report the degradation of synthetic dyes by Fenton-like reactions using Fe<sub>80</sub>P<sub>13</sub>C<sub>7</sub> amorphous ribbons for the first time, and the degradation processes using Fe<sub>78</sub>Si<sub>9</sub>B<sub>13</sub> amorphous ribbons are investigated for comparison. Methylene blue (MB), a common synthetic dye for ink production and textile coloring, is used as the degradation object in this work. The extremely long service life of FePC ribbons is revealed by cyclic tests. The underlying mechanism of the high degradation efficiency and the “self-renewing” characteristics of FePC amorphous ribbons in the Fenton-like reaction, as well as the

possible degradation pathways of MB are investigated. The effects of temperature, initial pH, initial H<sub>2</sub>O<sub>2</sub> concentration, ribbon dosage, and dye concentration on the degradation efficiency of MB using FePC amorphous ribbons during Fenton-like reactions are systematically studied. This work not only provides a new solution for wastewater remediation, but also extends the possible application areas of FePC amorphous alloys.

## Experimental

### Materials and reagents

Alloy ingots with a nominal composition of Fe<sub>80</sub>P<sub>13</sub>C<sub>7</sub> (at%) were prepared by induction melting of high-purity Fe (99.99 wt%), pre-alloyed Fe–P ingots (consisting of 75 at% Fe and 25 at% P) and Fe–C ingots (consisting of 96 at% Fe and 4 at% C) in an induction melting furnace, which was vacuumed to  $5 \times 10^{-3}$  Pa first and then filled with purified argon (99.999%). Alloy ingots with a nominal composition of Fe<sub>78</sub>Si<sub>9</sub>B<sub>13</sub> (at%) were prepared by arc melting of high-purity Fe (99.99 wt%), Si (99.99 wt%), and B (99.99 wt%) in an arc melting system, which was vacuumed to  $5 \times 10^{-3}$  Pa first and then filled with purified argon (99.999%). Ribbons with a thickness of  $\sim 25$   $\mu\text{m}$  and a width of  $\sim 2$  mm were prepared in a single roller melt-spinning system, which was vacuumed to  $5 \times 10^{-3}$  Pa first and then filled with purified argon (99.999%). The ribbons were obtained when the roller speed was 40 m s<sup>-1</sup>. The ribbons were cut into 1 cm long strips for degradation experiments. Commercially available synthetic dye (methylene blue, AR grade) was purchased from Xiya Reagent. Sodium hydroxide (NaOH, AR grade) was purchased from Greagent. Sulphuric acid (H<sub>2</sub>SO<sub>4</sub>, AR grade) was purchased from Chron Chemicals. Hydrogen peroxide (H<sub>2</sub>O<sub>2</sub>, AR grade) was purchased from Sinopharm Chemical Reagent Co., Ltd.

### Characterization

The amorphous structure of the as-quenched ribbons, which were fixed on slides using double-sided adhesive tapes, was verified by X-ray diffraction (XRD, Bruker D8 Discover) with Cu-K $\alpha$  radiation. The surface morphology and elemental information of the as-cast and reacted ribbons were observed using a scanning electron microscope (SEM, FEI Sirion 200) equipped with an energy dispersive X-ray spectrometer (EDS). Carbon tapes were used to fix the ribbons on the SEM sample holders. The binding states of elements on the surfaces of the as-cast and reacted FePC and FeSiB ribbons were evaluated by X-ray photoelectron spectroscopy (XPS, Thermo ESCALAB 250XI) with a monochromatic Al K $\alpha$  X-ray source ( $h\nu = 1486.6$  eV). The power was 150 W, and the X-ray spot size was set to be 500  $\mu\text{m}$ . The pass energy of the XPS analyzer was set at 20 eV. The base pressure of the analysis chamber was better than  $5 \times 10^{-9}$  Torr. The concentration of elements in the supernatant after batch reactions was measured using an inductively coupled plasma emission spectrometer (ICP, Spectroblue ICP-OES). The supernatant was obtained by filtering the extracted solution with a 0.22 mm membrane.

## Electrochemical tests

The electrochemical properties were analyzed using an electrochemical measuring instrument (Gamry Interface 1000). The measurements were conducted in a three-electrode cell using a platinum counter electrode and an Ag/AgCl reference electrode. The potential-dynamic polarization curves were recorded at a potential sweep speed of  $4 \text{ mV s}^{-1}$  after the open circuit potentials were stabilized. Electrochemical impedance spectroscopy (EIS) was conducted under static conditions with scanning frequencies from 100 kHz to 0.01 Hz and amplitude being 5 mV. The solution used for both the polarization measurements and EIS tests was 50 mL acid MB solution with  $\text{H}_2\text{O}_2$  (pH = 3, 1 mM  $\text{H}_2\text{O}_2$ , 100  $\text{mg L}^{-1}$  MB).

## Degradation experiments

250 mL MB solution ( $100 \text{ mg L}^{-1}$  if not noted) was prepared using deionized (DI) water in a 500 mL beaker. A specific amount of ribbons ( $0.5 \text{ g L}^{-1}$  if not noted) and  $\text{H}_2\text{O}_2$  (1 mM if not noted) were added to the solution, which was stirred at a fixed speed during the degradation process. The temperature (298 K if not noted) of the solution was maintained using a water bath. The initial pH (pH = 3 if not noted) of the solution was adjusted using 5%  $\text{H}_2\text{SO}_4$ , as well as 1 M and 0.1 M NaOH. At selected time intervals, 2.5 mL of the solution was extracted using a syringe and filtered with a 0.22  $\mu\text{m}$  membrane, and then scanned using a UV-Vis spectrophotometer (Shimadzu UV-1280) to obtain the absorbance spectrum of the solution. For cyclic tests, the ribbons were extracted from the solution after each degradation experiment and stir washed with DI water for 20 s before putting them into the next reaction batch.

## Results and discussion

### Comparison of the degradation efficiency using FePC and FeSiB amorphous ribbons

**Degradation performance at room temperature.** The amorphous nature of the as-cast  $\text{Fe}_{80}\text{P}_{13}\text{C}_7$  and  $\text{Fe}_{78}\text{Si}_9\text{B}_{13}$  ribbons is confirmed by XRD, because only broad diffuse peaks around  $45^\circ$  are observed (data not shown). According to previous research carried out by Wang *et al.*,  $\text{Fe}_{78}\text{Si}_9\text{B}_{13}$  amorphous ribbons have the best performance in decomposing rhodamine B at pH = 3, as Fenton-like reactions favor acidic solutions.<sup>18</sup> So we compared the degradation efficiency of FePC and FeSiB amorphous ribbons at pH = 3. Other reaction conditions are set as follows:  $T = 298 \text{ K}$ , initial  $\text{H}_2\text{O}_2$  concentration ( $C_{\text{H}_2\text{O}_2}$ ) = 1 mM, ribbon dosage =  $0.5 \text{ g L}^{-1}$ , initial MB concentration ( $C_{\text{MB}}$ ) =  $100 \text{ mg L}^{-1}$ . A decolorization phenomenon is observed during

the Fenton-like reaction using both FeSiB and FePC ribbons as shown in Fig. 1(a) and (b). The solution with FeSiB ribbons turns clear within 14 min, while that with FePC ribbons takes 11 min.

The UV-Vis absorbance spectra of the filtered MB solutions after adding FeSiB and FePC amorphous ribbons in the reaction batches for a series of time intervals are presented in Fig. 2(a) and (b), respectively. Four absorption peaks are observed for MB solutions at 247 nm, 291 nm, 618 nm and 653 nm. The peaks at 247 nm and 291 nm are from triazine groups, while the other two peaks at 618 nm and 653 nm represent auxochrome and chromophore groups, respectively.<sup>21</sup> All of these three peaks decrease gradually over the whole reaction process, corresponding to the concentration change of the MB solution and the visualized decolorization phenomenon as shown in Fig. 1. The normalized concentration of the MB solution is obtained with the peak values at 653 nm as they represent chromogenic species, as shown in Fig. 2(c). The concentration of the solutions reacting with both kinds of ribbons stays almost unchanged during the first 3 min, and then decline rapidly. The time required for the generation of  $\cdot\text{OH}$  groups and the  $\cdot\text{OH}$  groups approaching the dye molecules can be the reasons for the undiminished MB concentration at the beginning. According to the data derived from UV-Vis absorbance spectra, it takes 11 min for FePC ribbons to reduce  $C_t/C_0$  to less than 5% by the Fenton-like reaction, while it takes 14 min for FeSiB ribbons, which is consistent with the direct visual observation in Fig. 1. We take  $C_t/C_0 < 5\%$  (when 95% of MB is decomposed) as the degradation completion target for instrumental fluctuation in this paper. The degradation kinetics after the first 3 min are commonly described by the pseudo-first-order equation as given below:

$$C_t = C_0 \exp(-kt) \quad (5)$$

where  $k$  is the reaction rate constant ( $\text{min}^{-1}$ ),  $t$  is the reaction time (min),  $C_0$  is the initial concentration of MB ( $\text{mg L}^{-1}$ ), and  $C_t$  is the instant concentration of MB ( $\text{mg L}^{-1}$ ) at time  $t$ . Then the degradation reaction rate constant can be derived as follows:

$$k = \ln\left(\frac{C_0}{C_t}\right) / t \quad (6)$$

According to the  $\ln(C_0/C_t)$  vs.  $t$  curve shown in Fig. 2(d), the reaction rate constant of FePC ribbons in this Fenton-like reaction is  $0.56 \text{ min}^{-1}$ , which is larger than  $0.37 \text{ min}^{-1}$  for FeSiB ribbons, with the goodness of fit  $R^2$  being 0.96 and 0.98,

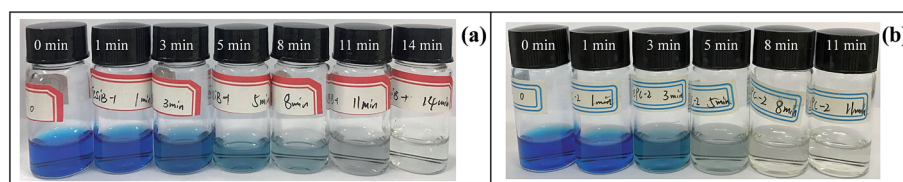


Fig. 1 Visible colour change of MB solutions during Fenton-like reactions using (a) FeSiB and (b) FePC amorphous ribbons.

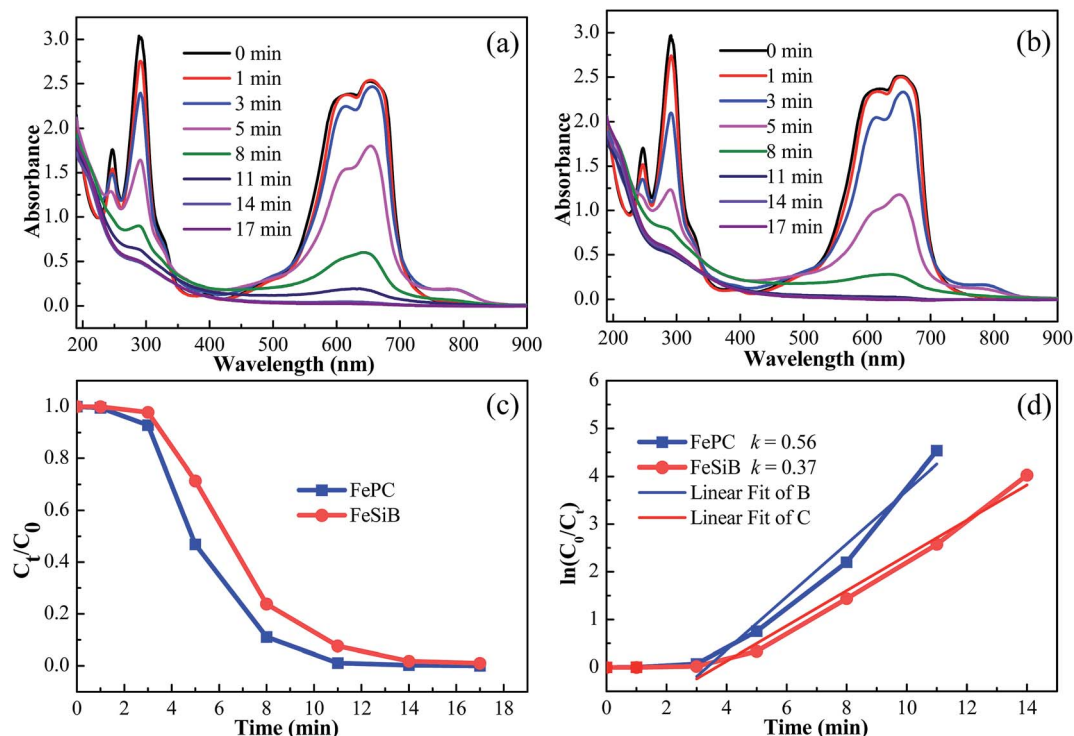


Fig. 2 UV-Vis absorbance spectra of MB solutions during the Fenton-like reactions using (a) FeSiB and (b) FePC amorphous ribbons; (c) normalized concentration change of MB solutions during the degradation process; (d) the  $\ln(C_0/C_t)$  vs. time curves for FePC and FeSiB amorphous ribbons ( $T = 298$  K,  $\text{pH} = 3$ ,  $C_{\text{H}_2\text{O}_2} = 1$  mM, ribbon dosage =  $0.5$  g  $\text{L}^{-1}$ ,  $C_{\text{MB}} = 100$  mg  $\text{L}^{-1}$ ).

respectively. Based on the above results, it can be concluded that FePC amorphous ribbons exhibit excellent ability in MB degradation by the Fenton-like reaction, even better than FeSiB amorphous ribbons. One may have a query about the practicability of FePC ribbons in wastewater remediation as P may leak into the solution during the reaction. To dispel this doubt, we performed ICP analysis of the filtered solution after degradation and found out that the P concentration is below the instrument detection limit of 0.0107 ppm, which is far below the primary level of the integrated wastewater discharge standard of People's Republic of China (GB 8978-1996). The degradation experiments were repeated more than 3 times to assure the authenticity of the results.

**Reaction activation energy.** To further compare the degradation efficiency of Fenton-like reactions using FePC and FeSiB ribbons, the thermal activation energy of MB degradation using corresponding ribbons is analyzed by carrying out the reactions at different temperatures, as shown in Fig. 3. The reaction conditions are set as follows: initial  $\text{pH} = 3$ ,  $C_{\text{H}_2\text{O}_2} = 1$  mM, ribbon dosage  $0.5$  g  $\text{L}^{-1}$ , and  $C_{\text{MB}} = 100$  mg  $\text{L}^{-1}$ . The normalized concentration change of MB reveal the positive influence of temperature on the degradation process, as the decolorization process takes less time with an increased solution temperature [Fig. 3(a) and (b)]. Raising the temperature accelerates the Fenton reaction process, which increases the generation rate of the  $\cdot\text{OH}$  group, thus the decolorization efficiency is enhanced. MB solutions are completely decolorized in solutions with FeSiB and FePC ribbons within 8 min, 5 min and 3 min at 308 K, 318 K and 328 K, respectively. The required completion time for

degradation processes is similar at higher temperature. However, difference in the reaction kinetics can still be found when evaluating the reaction rate constants at different temperatures for FePC and FeSiB amorphous ribbons. When the solution temperature increases from 298 K to 308 K, 318 K and 328 K, the degradation rate constant of FePC ribbons increases from  $0.56$   $\text{min}^{-1}$  to  $0.58$   $\text{min}^{-1}$ ,  $0.90$   $\text{min}^{-1}$  and  $1.24$   $\text{min}^{-1}$ , while that of FeSiB ribbons increases from  $0.37$   $\text{min}^{-1}$  to  $0.44$   $\text{min}^{-1}$ ,  $0.86$   $\text{min}^{-1}$  and  $1.24$   $\text{min}^{-1}$ , respectively [Fig. 3(c)]. It is noticed that the reactivity of the solution with FeSiB ribbons increases more rapidly than that with FePC ribbons when the temperature increases, and even reaches the same performance at 328 K. This may be because the huge improvement of the generation rate of the  $\cdot\text{OH}$  group in the Fenton reaction with increased temperature has eliminated the difference of the  $\text{Fe}^{2+}$  production rate between the two types of ribbons.

As the reaction rate is highly affected by temperature, we can derive the thermal activation energy for the degradation of MB using Fenton-like reactions with FePC and FeSiB ribbons by using the Arrhenius-type equation:

$$\ln k_T = -\frac{\Delta E}{RT} + \ln A \quad (7)$$

where  $k_T$  is the reaction rate constant at different temperatures,  $\Delta E$  is the reaction activation energy,  $R$  is the gas constant and  $A$  is a constant. We plotted  $\ln k_T$  vs.  $-1/RT$  as shown in Fig. 3(d) and found that the reaction activation energies of FePC and FeSiB ribbons are  $22.8$  kJ  $\text{mol}^{-1}$  and  $34.8$  kJ  $\text{mol}^{-1}$ , respectively.

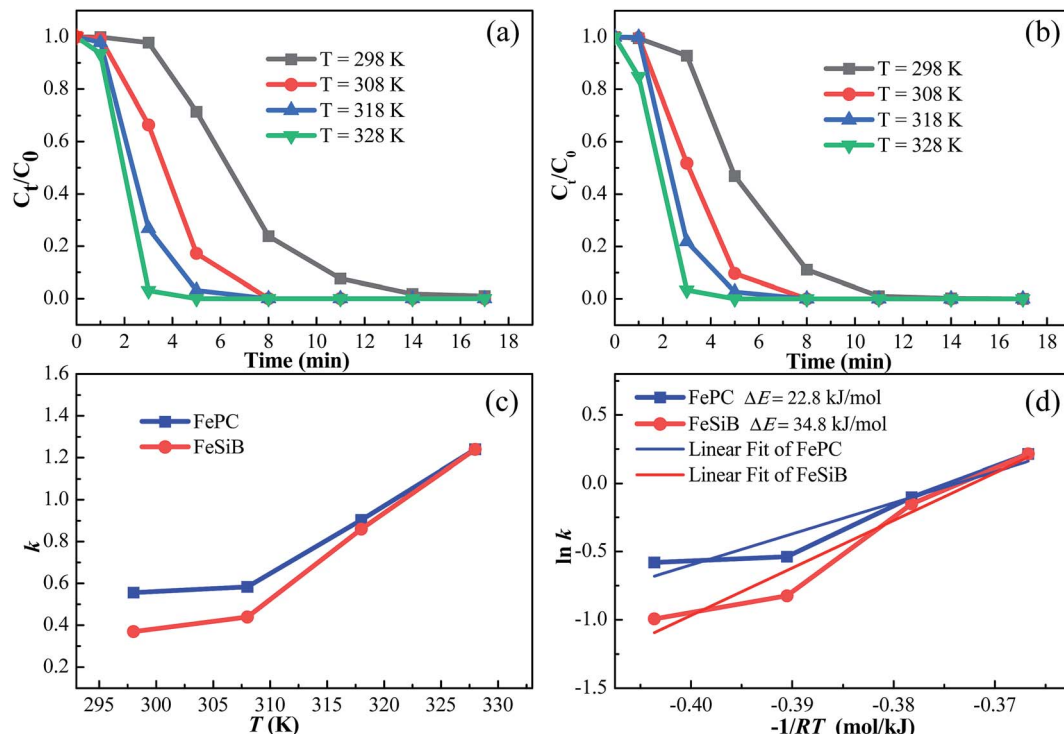


Fig. 3 Normalized concentration change of MB solutions during the Fenton-like reactions using (a) FeSiB and (b) FePC amorphous ribbons at different temperatures; (c) derived reaction rate constants  $k$  at different reaction temperatures; (d)  $\ln k$  vs.  $-1/RT$  curves for FePC and FeSiB amorphous ribbons (pH = 3,  $C_{H_2O_2}$  = 1 mM, ribbon dosage = 0.5 g L<sup>-1</sup>,  $C_{MB}$  = 100 mg L<sup>-1</sup>).

The lower activation energy of FePC ribbons contributes to their better performance in the Fenton-like reaction.

### Mechanism studies of the degradation processes using FePC and FeSiB amorphous ribbons

**Surface morphology.** As the degradation process is surface-mediated, it is crucial to understand the structural change on the surface of the ribbons during the Fenton-like reaction. SEM and EDS analyses on the surface of the as-cast and reacted FeSiB and FePC ribbons are compared in Fig. 4. A typical smooth surface of amorphous ribbons is observed on the as-cast FeSiB and FePC ribbons in Fig. 4(a) and (b) respectively. 3D nanoporous structures present on the reacted FeSiB ribbon, [Fig. 4(c)], are consistent with the reported morphology for the reacted FeSiB and FeSiB-based alloys.<sup>15,20,48</sup> These structures have been proposed to have positive effects during the decolorization process as they provide channels for mass transfer. Similar 3D nanoporous structures, with more open pores than those on the reacted FeSiB ribbon, are found to be spread all over the reacted FePC ribbon in Fig. 4(d). The relatively higher density of pores may be the reason for the higher performance of FePC ribbons in Fenton-like reactions.

The EDS results of the surface of the as-cast and reacted FeSiB and FePC ribbons are summarized in Table 1. Boron is too light to be quantitatively analyzed by EDS, and the amount of carbon is not accurate either, due to sample handling and the carbon paste for sample fixation. So we tracked the amount of oxygen, as well as the Fe/Si ratio of the FeSiB ribbon and the

Fe/P ratio of the FePC ribbon for elemental analysis. The amount of oxygen on the surface of both as-cast ribbons is too small to be detected, but increases to 16.7 at% on the reacted FeSiB ribbon, and 18.6 at% on the reacted FePC ribbon, revealing that the oxidation of the ribbons is involved during the degradation process. The Fe/Si ratio and the Fe/P ratio of as-cast ribbons are  $\sim 8.0$  and  $\sim 6.0$ , respectively, which are close to the nominal composition of Fe<sub>78</sub>Si<sub>9</sub>B<sub>13</sub> and Fe<sub>80</sub>P<sub>13</sub>C<sub>7</sub> ribbons. The amount of iron in both ribbons decreases after the degradation experiment, as the Fe/Si ratio drops to  $\sim 6.8$ , and the Fe/P ratio drops to  $\sim 3.6$ , respectively. The zero-valent iron from the ribbon surface react with H<sub>2</sub>O<sub>2</sub> to provide  $\cdot$ OH, and transform into iron oxides or iron hydroxides, which are soluble in the acidic solution. Thus, similar to the reported FeSiB/FeSiB-based amorphous alloys, the remaining phosphate and carbon in FePC ribbons form the 3D nanoporous structures, which is beneficial to the degradation efficiency as they provide channels for mass transport. Besides, carbon itself possesses large adsorption ability of organics, which accelerates the MB approaching FePC ribbons.<sup>45</sup>

**Electronic structure.** As shown in eqn (1)–(3), the electronic structure change of Fe<sup>0</sup> and Fe<sup>2+</sup> controls the generation speed of  $\cdot$ OH, which has a great impact on the degradation efficiency. To understand the mechanism of the higher degradation performance of FePC ribbons, the electronic structure of the two kinds of ribbons during the degradation process is compared.

In order to obtain information on the electronic structure of the surface of FePC ribbons before and after degradation, XPS

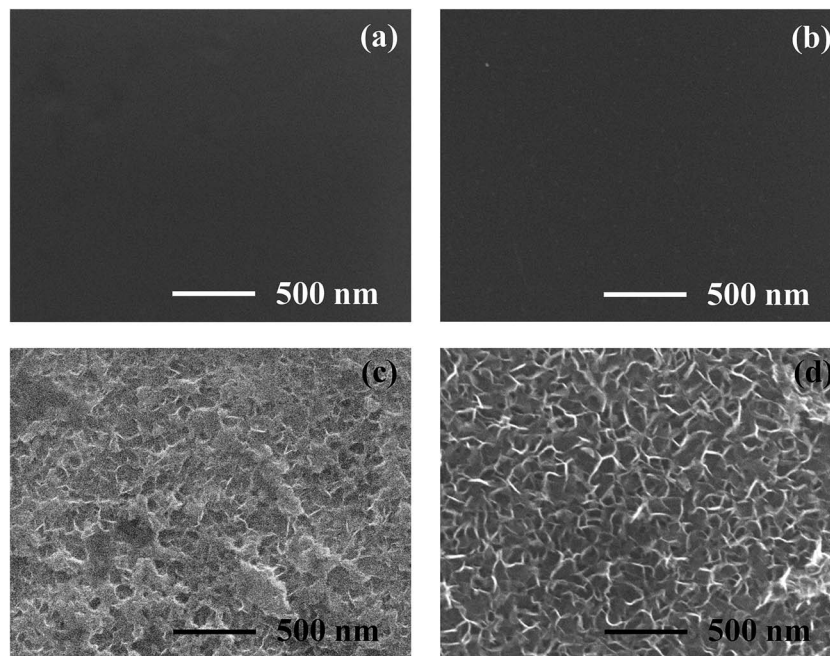


Fig. 4 SEM micrographs of (a) as-cast FeSiB ribbon, (b) as-cast FePC ribbon, (c) reacted FeSiB ribbon and (d) reacted FePC ribbon.

Table 1 EDS analysis of the as-cast and reacted FePC and FeSiB ribbons (at%)

	Fe	P	C	O	Si	B
As-cast FeSiB ribbon	47.9	—	1.6	—	5.9	44.6
FeSiB ribbon after 1 cycle	33.5	—	3.9	16.7	4.9	41.0
FeSiB ribbon after 7 cycles	32.5	—	5.6	17.4	6.5	38.0
As-cast FePC ribbon	65.5	11.0	23.5	—	—	—
FePC ribbon after 1 cycle	39.2	11.0	31.2	18.6	—	—
FePC ribbon after 7 cycles (top layer)	12.7	7.1	43.2	37.0	—	—
FePC ribbon after 7 cycles (main part)	31.9	16.0	19.9	32.2	—	—

analysis was performed on the surface of the as-cast and reacted ribbons over a wide binding range to measure Fe  $2p_{3/2}$ , P  $2p$ , C  $1s$  and O  $1s$ . As shown in Fig. 5(a), the Fe  $2p_{3/2}$  spectrum is deconvoluted into 3 peaks, including peaks at 707.0 eV, 710.5 eV and 711.2 eV. The 707.0 eV peak is assigned to the metallic state Fe<sup>0</sup>, while the peaks at 710.5 eV and 711.2 eV are both from the oxidized Fe<sup>2+</sup>/Fe<sup>3+</sup> ions.<sup>49</sup> The area under each peak is related to its intensity. The relative amount of the investigated elements at different electronic states can be calculated based on the areas of the peaks. Not much difference in the Fe<sup>0</sup>/Fe<sup>2+</sup>(Fe<sup>3+</sup>) amount ratio is observed for the ribbons before and after the reaction, while the total amount of iron on the surface of the reacted ribbon is much lower than that of the as-cast one, confirming that iron participates in the degradation of MB, which is consistent with the EDS results in Table 1. The O  $1s$  spectrum obtained on the surface of the as-cast FePC ribbon consists of 2 peaks at 530.0 eV and 531.6 eV, as shown in Fig. 5(b), which are assigned to the oxygen bound to iron and the oxygen bound to phosphate/carbon, respectively.<sup>50,51</sup> The O  $1s$  spectrum obtained from the surface of the reacted ribbon can be deconvoluted into 4 peaks, with the peak at 530.0 eV related to the oxygen bound to

iron, and all other three peaks at 531.6 eV, 532.1 eV and 532.5 eV assigned to the oxygen bound to phosphate/carbon. Compared to the as-cast ribbon, the surface of the reacted ribbon contains more oxygen bound to phosphate/carbon, and less oxygen bound to iron, which is in agreement with the loss of iron from the Fe  $2p_{3/2}$  spectrum.

Both of the C  $1s$  spectra from the as-cast and reacted ribbons consist of 3 peaks at 284.6 eV, 285.3 eV and 288.4 eV, as shown in Fig. 5(c). The peaks at 284.6 eV and 285.3 eV are from C<sup>0</sup>, while the peak at 288.4 eV is from “-C=O-” bonds.<sup>52,53</sup> The amount of carbon that form C<sup>0</sup> is about 87% of the total carbon on the surface of the as-cast FePC ribbon, and decreases to ~70% after degradation, which means that ~17% of C changes from the zero-valent state to the oxidized state. For P  $2p$  spectra in Fig. 5(d), the peaks at 129.3 eV and 130.0 eV are assigned to P<sup>0</sup>, and the peak at 133.2 eV is assigned to P<sup>5+</sup>.<sup>54</sup> The P<sup>0</sup>/total P ratio decreases from 62% for the as-cast ribbon to 29% for the ribbon after degradation. In other words, ~33% P changes from the zero-valent state to the oxidized state.

As Zhou *et al.* revealed that FePC amorphous alloys are mostly composed of P-centered antiprism-like and C-centered

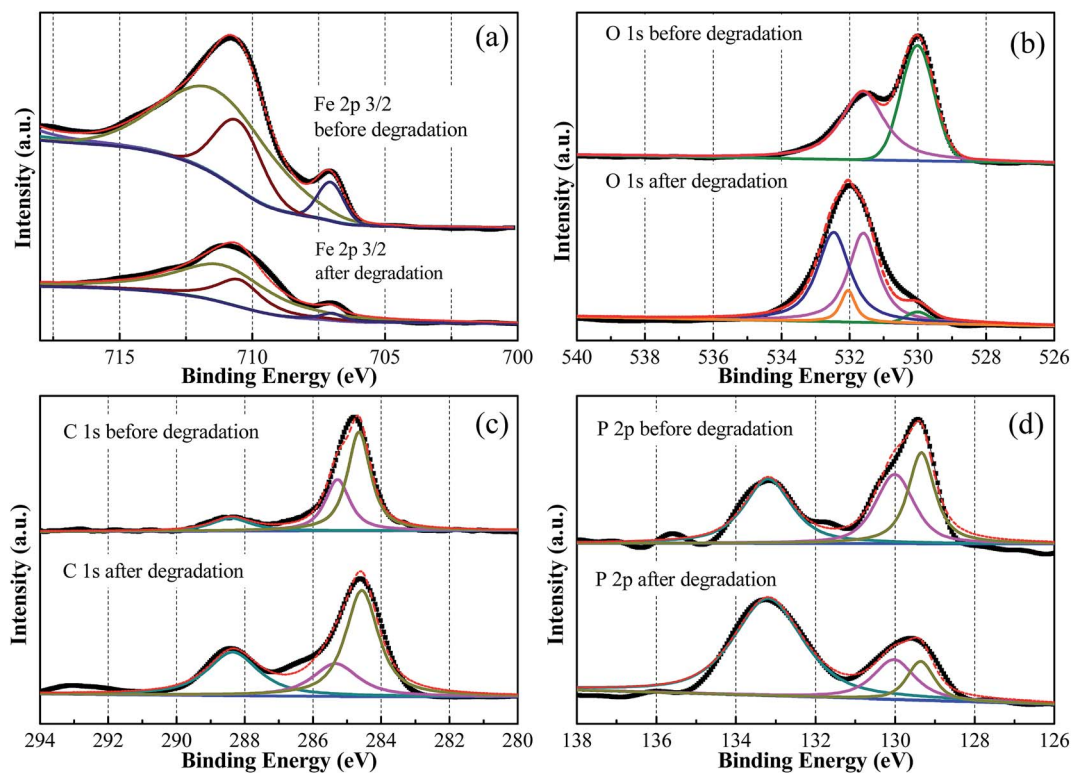


Fig. 5 XPS spectra of (a) Fe  $2p_{3/2}$ , (b) O 1s, (c) C 1s and (d) P 2p in binding energy regions for the FePC amorphous ribbons before and after degradation.

prism-like clusters, without metalloids occupying the nearest-neighbor sites of each other, providing a large amount of Fe–P and Fe–C bonds,<sup>55</sup> we may propose that the loss of C<sup>0</sup> and P<sup>0</sup> results from the breakage of Fe–C and Fe–P bonds. The percentage of the Fe–P bond breakage is almost twice that of the Fe–C bond breakage. This can be explained as the bond strength of Fe–P is lower than that of Fe–C as the bond length of Fe–P is longer.<sup>40</sup> It is quite possible that the strong Fe–C bonds and the weak Fe–P bonds in FePC amorphous ribbons form galvanic cells, leading to the fast dissolution of iron in MB solution, which explains the advanced degradation performance of the Fenton-like reaction using FePC amorphous ribbons.

The electronic structure of the as-cast and reacted FeSiB amorphous ribbons is also obtained using XPS for comparison as shown in Fig. 6. Similar to the iron in FePC ribbons, the spectrum of Fe  $2p_{3/2}$  in the as-cast FeSiB ribbon is deconvoluted into three peaks, with one peak at 706 eV representing the metallic state Fe<sup>0</sup>, and other two peaks at 710.0 eV and 710.8 eV assigned to the oxidized Fe<sup>2+</sup>/Fe<sup>3+</sup> ions, as shown in Fig. 6(a). The peak of Fe<sup>0</sup> completely disappears and the total amount of Fe drops a lot in the spectrum of the reacted FeSiB ribbon, confirming the participation of Fe in the Fenton-like reaction. For O 1s, the spectrum of the as-cast ribbon is deconvoluted into three peaks, with 29.8 eV from Fe–O bonds, and 530.7 eV and 531.7 eV from Si–O and B–O bonds [Fig. 6(b)]. Corresponding peaks also appear in the O 1s spectrum of the reacted FeSiB ribbon, while all the peaks shift to higher binding energy.

Obvious increase in the areas of the peaks representing Si–O and B–O bonds is observed, together with the decrease of the area under the Fe–O peak, which is in agreement with the loss of the total iron from the Fe  $2p_{3/2}$  spectra.

The spectra of the measured Si 2p from the as-cast and reacted FeSiB ribbons are presented in Fig. 6(c). For the as-cast ribbon surface, the Si 2p spectrum is deconvoluted into four peaks: the peaks located at 98.9 eV and 99.5 eV are assigned to Si<sup>0</sup>, and the two peaks located at 101.4 eV and 102.0 eV are assigned to the oxidized Si<sup>4+</sup> ions.<sup>49</sup> For the reacted ribbon surface, the two peaks corresponding to Si<sup>0</sup> disappear. Instead, a weak peak located at 99.3 eV representing Si<sup>0</sup>, together with two Si<sup>4+</sup> peaks, is observed in the spectrum. The Si<sup>0</sup>/Si<sub>total</sub> ratios calculated from the spectra of the as-cast and reacted ribbons are ~30% and ~1%, respectively. It is then reasonable to conclude that ~29% of Si atoms transform from the Si<sup>0</sup> state to the Si<sup>4+</sup> state. Both of the B 1s spectra from the as-cast and reacted FeSiB ribbons consist of two peaks located at 187.5 eV and 191.8 eV corresponding to B<sup>0</sup> and B<sup>3+</sup> states, respectively.<sup>49</sup> The B<sup>0</sup>/B<sub>total</sub> ratio decreases from ~40% for the as-cast ribbon to ~10% for the reacted ribbon. Thus, ~30% of B atoms transform from the B<sup>0</sup> state to the oxidized B<sup>3+</sup> state, which is very close to the amount of the oxidized Si atoms. Apparently, no galvanic cell phenomenon is observed for FeSiB ribbons, which may explain their relatively low performance in the Fenton-like reaction.

Furthermore, two characteristics of the electronic structures of FeSiB alloys may explain their relatively low efficiency in

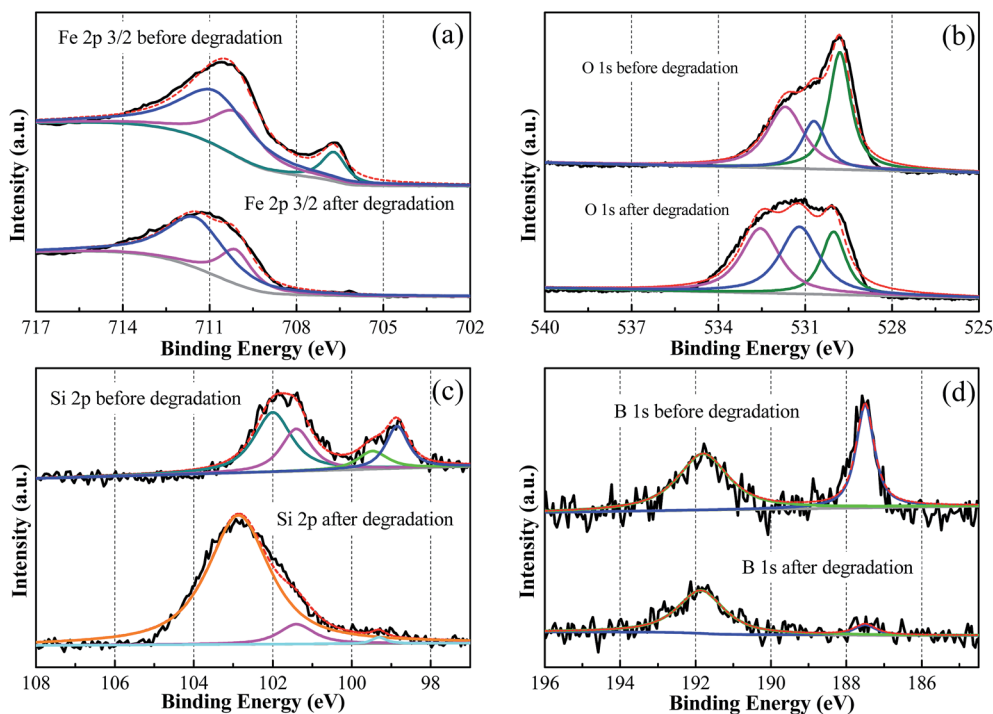


Fig. 6 XPS spectra of (a) Fe  $2p_{3/2}$ , (b) O 1s, (c) Si 2p and (d) B 1s in binding energy regions for the FeSiB amorphous ribbons before and after degradation.

Fenton-like reactions.<sup>55–58</sup> First of all, calculations of FeSiB amorphous alloys revealed that the nearest-neighbor sites of metalloids are not only occupied by Fe atoms, but also by a small amount of other metalloids, forming solute–solute contacts that is not in favor of the formation of galvanic cells.<sup>55</sup> Secondly, like carbon in FePC, all the boron atoms stay in the B-centered prism-like clusters in FeSiB. However, different from the P-centered antiprism-like structures in FePC, a bcc-like Fe–Si solid-solution forms in FeSiB with Si atom solid-dissolved in the Fe matrix.<sup>56</sup> The Fe–Si solid solution structure is more stable than metal–metalloid clusters as the primary crystalline phase of an annealed FeSiB amorphous alloy is  $\alpha$ -Fe(Si), instead of  $\alpha$ -Fe crystals for most of the Fe-based amorphous alloys without Si addition, including the FePC system.<sup>57,58</sup> It is more difficult for the zero valent iron to escape from the solid solution structure to participate in the degradation reaction. Thus, the solute–solute contacts and the Fe–Si solid solution together may explain the relatively poor degradation performance of Fenton-like solutions with FeSiB ribbons.

Based on the surface morphology and the electronic structure analyses, the densely distributed nanoporous structures, together with the galvanic cells formed between Fe–P and Fe–C bonds, contribute to the excellent performance of FePC amorphous ribbons in Fenton-like reactions.

#### Comparison of the stability and reusability of FePC and FeSiB amorphous ribbons

**Long service life.** The reusability of amorphous ribbons is of great importance when evaluating their potential for wastewater

remediation. FeSiB amorphous ribbons are reported to be applicable for 4 cycles when participating in Fenton-like reactions, and 10 cycles when activating peroxymonosulfate in the degradation of naphthol green B.<sup>21,59</sup> Fenton-like reactions using FeSiB amorphous ribbons that we synthesized in this study are capable of decomposing 95% of MB within 17 min for 8 cycles, but with a small drift during cycle 4, as shown in Fig. 7(a) and (c). However in the 9th cycle, it takes more than 20 min for the solution to finish degradation.

Surprisingly, Fenton-like reactions with FePC ribbons synthesized in this work are capable of degrading 95% of MB within 14 min for 19 cycles [Fig. 7(b) and (d)]. One may notice that the degradation processes of the 2nd and 3rd cycles for FePC ribbons finish within 8 min, even faster than that for the 1st cycle when the ribbon is freshly prepared. This may be because it takes more time to consume the thin oxide layer on the ribbon during the first test, while the 2nd and 3rd run enjoy truly “fresh” surfaces of FePC amorphous ribbons. After three degradation cycles, the amount of available zero valent iron on the ribbon surface decreases, so the required degradation time from the 4th to the 8th cycles increases to 14 min. The degradation processes are extended to 17 min for the 9th and 10th cycles, as a large amount of iron has been consumed by then. However, the degradation ability of FePC ribbons using Fenton-like reactions recovers to  $t_{95\%} = 14$  min from cycle 11 to 19. The mechanism of this unusual recovery will be discussed with surface morphology analysis later.

**Corrosion property.** The corrosion process usually occurs at the heterogeneous sites of crystalline materials, including second phases, grain boundaries, dislocations, *etc.* However,

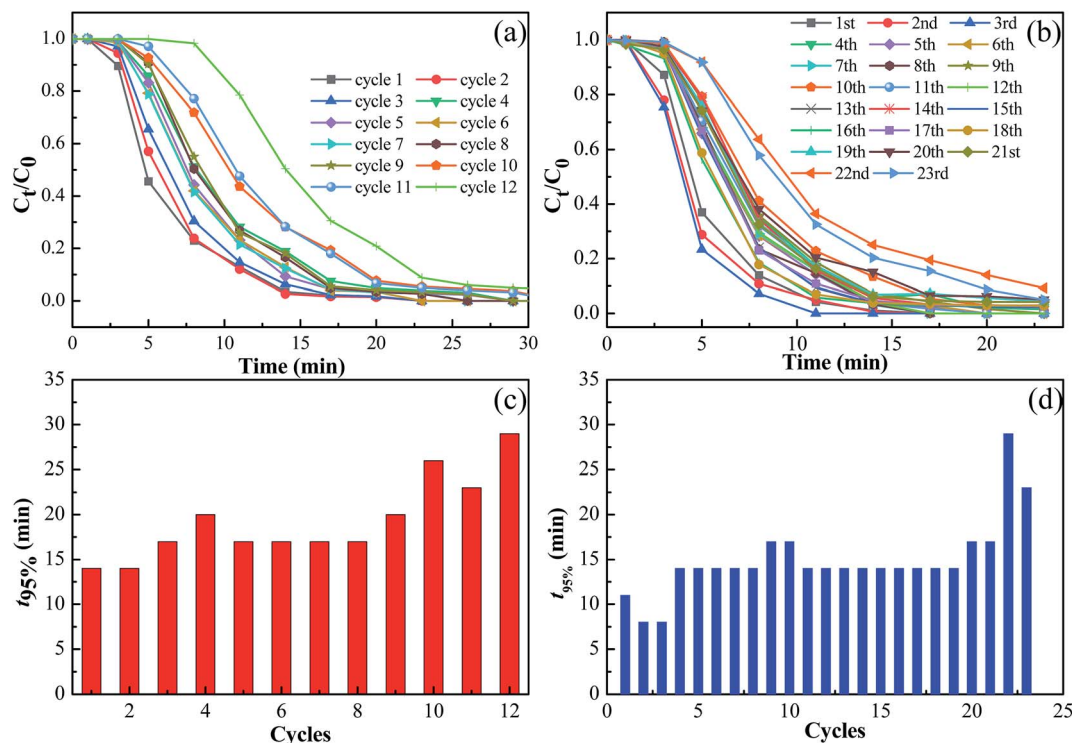


Fig. 7 (a) Normalized concentration change of MB solutions during the Fenton-like reactions using FeSiB ribbons from the 1st to the 12th degradation cycles; (b) normalized concentration change of MB solutions during the Fenton-like reactions using FePC ribbons from the 1st to the 23rd degradation cycles; (c) the time required for 95% completion of the degradation process vs. reaction cycles for FeSiB ribbons; (d) time required for 95% completion of the degradation process vs. reaction cycles for FePC ribbons ( $T = 298$  K,  $\text{pH} = 3$ ,  $C_{\text{H}_2\text{O}_2} = 1$  mM, ribbon dosage =  $0.5$  g  $\text{L}^{-1}$ ,  $C_{\text{MB}} = 100$  mg  $\text{L}^{-1}$ ).

amorphous alloys formed by rapid quenching are composed of a single phase of homogenous solid solution without any physical or chemical heterogeneity. Thus, amorphous alloys are superior in corrosion resistance compared to their crystalline counterparts.<sup>60</sup> The service life of amorphous ribbons for degradation application is believed to be related to their corrosion resistance, as the oxidized layer may impede the electron transfer from  $\text{Fe}^0$  to the solution.<sup>21</sup> Thus, the corrosion properties of the as-cast FePC and FeSiB amorphous ribbons are compared.

Polarization curves and electrochemical impedance spectroscopy (EIS) results of the FePC and FeSiB amorphous ribbons in MB solution ( $\text{pH} = 3$ ,  $1$  mM  $\text{H}_2\text{O}_2$ ,  $100$  mg  $\text{L}^{-1}$  MB) are shown in Fig. 8. The passive potential of the FePC ribbon is  $-0.48$  V, which is higher than  $-0.63$  V for the FeSiB ribbon [Fig. 8(a)]. Besides, the passive current density of the FePC ribbon is  $1.26 \times 10^{-6}$  A  $\text{cm}^{-2}$ , which is lower than  $4.5 \times 10^{-6}$  A  $\text{cm}^{-2}$  for the FeSiB ribbon. The above data from polarization curves reveal the better corrosion performance for the FePC amorphous ribbon in acidic MB solution with  $\text{H}_2\text{O}_2$ .

The Nyquist plots derived from EIS analysis are shown in Fig. 8(b). The plots of both the FePC and FeSiB amorphous ribbons exhibit one time constant, while the FePC amorphous ribbon shows a larger capacitance loop than the FeSiB amorphous ribbon. An equivalent circuit model fitting the Nyquist plots is also presented in Fig. 8(b), with a constant phase

element (CPE) replacing an ideal capacitor to compensate for the surface inhomogeneity.  $R_1$  and  $R_2$  are the resistances of the solution, and the polarization resistance of ribbons, respectively. According to the fitted results, the polarization resistance of FePC and FeSiB ribbons are  $260$   $\Omega$   $\text{cm}^2$  and  $210$   $\Omega$   $\text{cm}^2$ , respectively, implying the better corrosion resistance for the FePC sample in acidic MB solution with  $\text{H}_2\text{O}_2$ , which is consistent with the results from the polarization curves.

The better corrosion resistance of FePC amorphous ribbons than FeSiB amorphous ribbons can be expected as Dan *et al.* pointed out that P addition could improve the corrosion resistance of Fe-based amorphous alloys due to the low-soluble iron phosphate compounds formed on the surface.<sup>61</sup>

The good corrosion resistance of FePC ribbons seems to conflict with their long service life. However, the corrosion property is only one of the influential factors of the reusability of FePC ribbons, and it may not be the decisive one. Microstructure analysis will be performed to reveal the mechanism of the excellent performance of FePC ribbons for the 19 reaction cycles, as shown below.

**“Self-renewing” behaviour.** Surface morphology is crucial not only for the degradation efficiency, but also for the reusability of the amorphous ribbons. To explain the extremely long service life of FePC amorphous ribbons in Fenton-like reactions, the surface morphology changes of FePC ribbons during cyclic tests are thoroughly analyzed (Fig. 9).

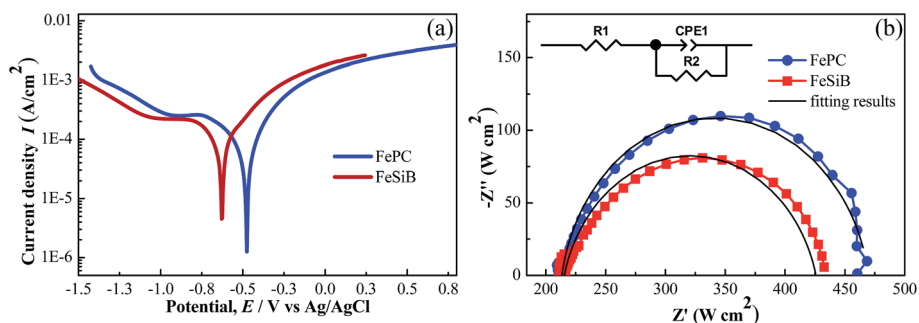


Fig. 8 Electrochemical behaviour of FePC and FeSiB amorphous ribbons in MB solutions ( $T = 298$  K,  $\text{pH} = 3$ ,  $\text{C}_{\text{H}_2\text{O}_2} = 1$  mM), (a) polarization curves; (b) Nyquist plots derived from EIS measurements.

A thin layer falling off from the ribbon surface is captured by SEM from the side view of FePC ribbons that have participated in the degradation processes for 7 cycles [Fig. 9(a)]. Close observation of the falling off layer is shown in the red square. The top view of the falling-off layer and the main part of the ribbon show a cotton-like structure and a 3D nanoporous structure, as shown in the blue and yellow ellipses, respectively. The EDS results of these two types of structures reveal that the atomic percentage of iron in the falling-off layer

is only 12.7%, which is much less than 31.9% for the main part, as listed in Table 1. Based on these results, it is reasonable to propose that the first 7 cycles may have consumed most of the iron on the top layer of the FePC ribbon and the relatively loose cotton-like structure forms on the surface of the ribbon. Then the top layer falls off gradually and the “fresh” FePC surface underneath gets a chance to participate in the Fenton-like reaction. This may explain the hump around cycles 9 and 10 in Fig. 7(d).

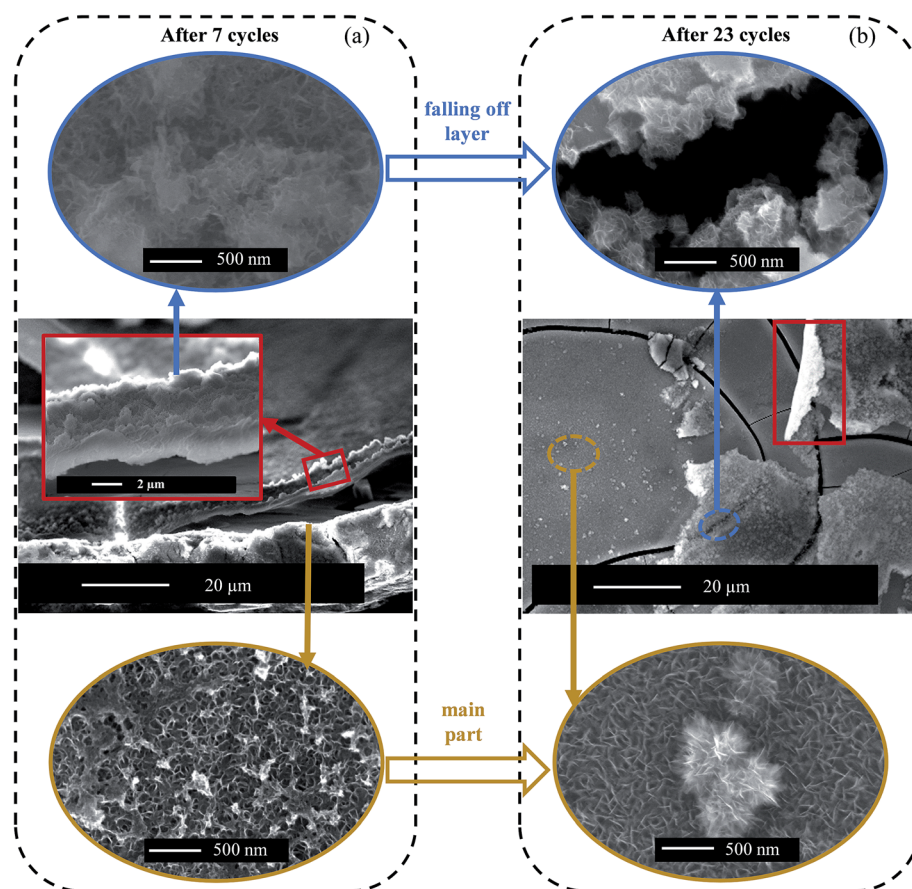


Fig. 9 SEM micrographs of FePC amorphous ribbons, (a) side view after 7 reaction cycles, with the enlarged “falling-off” layer highlighted by a red square, and top view of the “falling-off” layer and the main part presented in the blue and yellow ellipses respectively; (b) top view of the FePC ribbon after 23 reaction cycles, with the “falling-off” layer highlighted by a red square, and the enlarged “falling-off” layer and the main part presented in the blue and yellow ellipses respectively.

After 19 cycles, the degradation ability of the ribbons decreases rapidly due to the visible mass loss of the ribbons. Cyclic tests are dropped after 23 rounds since it is difficult to collect the ribbons by then due to the shattering of the samples. The surface morphology of FePC ribbons after 23 experimental cycles is investigated using SEM, as shown in Fig. 9(b). Loose flakes distribute on the cracked but relatively compact main part, with a titling flake highlighted by a red square. The difference between the thermal expansions of the original FePC ribbons and the reacted layer causes the cracks on the main part. Enlarged micrographs of the flakes and the main part are presented in the blue and yellow ellipses, showing similar loose cotton-like and 3D nanoporous structures as the falling-off layer and the main part of the ribbon after 7 reaction cycles, confirming the continual “self-renewing” behaviour of FePC ribbons during Fenton-like reactions. This “self-renewing” behaviour drives the exfoliation of the formed oxidized layer, which assures the long service life of FePC ribbons although they present high corrosion resistance under the previous electrochemical tests.

For comparison, the surface morphology of the FeSiB ribbon after 7 reaction cycles is also analyzed using SEM. The side view of the ribbon reveals that the surface is relatively compact, as shown in Fig. 10(a). The top view of the ribbon in Fig. 10(b) presents several cracks on the surface, which is the typical morphology of the oxidized passivation layer during corrosion as the thermal expansion coefficients of the oxides and the original alloy are different. The enlarged area, as shown in the yellow square, reveals that there is a small amount of nanoporous structures near the cracks. No “falling off” layer is observed within any analyzed field. The EDS results of the surface of the FeSiB ribbon after 7 reaction cycles are listed in Table 1. The Fe/Si ratio decreases to  $\sim 5.0$  after 7 reaction cycles, which is reasonable as the metallic iron continuously participates in the Fenton-like reaction. The comparison of the surface morphology between FePC and FeSiB ribbons during multiple reaction cycles reveals that the “self-renewing” behaviour is only observed for FePC amorphous ribbons, which may be the main reason for their extremely long service life during Fenton-like reactions.

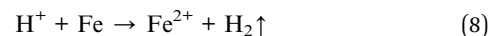
From the electronic structure perspective, the nearest neighbor sites of the metalloids in FePC amorphous alloys are only occupied by iron, while FeSiB amorphous alloys contain not only metal-metalloid bonds, but also a large amount of

metalloid-metalloid bonds. As a result, after the dissolution of iron atoms, the bonding between the oxidized layer and the original alloy in the FePC ribbon is not as strong as in the FeSiB ribbon. This may explain why the “self-renewing” behaviour only appears in the FePC alloy, not in the FeSiB alloy.

Apparently, both the “self-renewing behaviour” arising from the exfoliation of the oxidized layers, and the corrosion properties, influence the service life of FePC amorphous alloys, while the former is the determining factor in this case. Thus, the better reusability of FePC amorphous ribbons with higher corrosion resistance can be elucidated.

### Evaluation of the degradation performance of FePC ribbons under different reaction conditions

**Effect of pH.** The working pH range of the Fenton-like reaction using FePC ribbons for the MB degradation has been evaluated, while keeping other reaction conditions constant:  $T = 298\text{ K}$ ,  $C_{\text{H}_2\text{O}_2} = 1\text{ mM}$ , ribbon dosage =  $0.5\text{ g L}^{-1}$  and  $C_{\text{MB}} = 100\text{ mg L}^{-1}$ . As shown in Fig. 11(a), the highest reaction rate for FePC ribbons is achieved at  $\text{pH} = 3$ , same as reported for FeSiB ribbons. Surprisingly, the decolorization process finishes after 20 min at  $\text{pH} = 2$ , which is slower than that at  $\text{pH} = 3$ . This may be because when the concentration of  $\text{H}^+$  is too high in the solution, the iron from the ribbon will be dissolved to generate hydrogen as shown below:



This hydrogen evolution reaction produces a large amount of  $\text{Fe}^{2+}$ , which may consume a certain amount of  $\cdot\text{OH}$  (as eqn (4) shows) and lower the oxidation capability of the solution.

When  $\text{pH} > 3$ , the degradation efficiency of the solution decreases with the increasing pH, as enough  $\text{H}^+$  in the solution is essential for Fenton-like reactions. When the pH increases to 4 and 5, it takes 30 min and 180 min for the ribbons to complete the degradation process, respectively. In neutral ( $\text{pH} = 7$ ) and alkaline ( $\text{pH} = 9$ ) solutions, the decomposition of MB is rarely observed within 180 min.

**Effect of  $\text{H}_2\text{O}_2$  concentration.** The  $\text{H}_2\text{O}_2$  concentration controls the  $\cdot\text{OH}$  generation rate for the Fenton and Fenton-like reactions. The effect of the  $\text{H}_2\text{O}_2$  concentration on the decolorization process of MB using FePC amorphous ribbons is

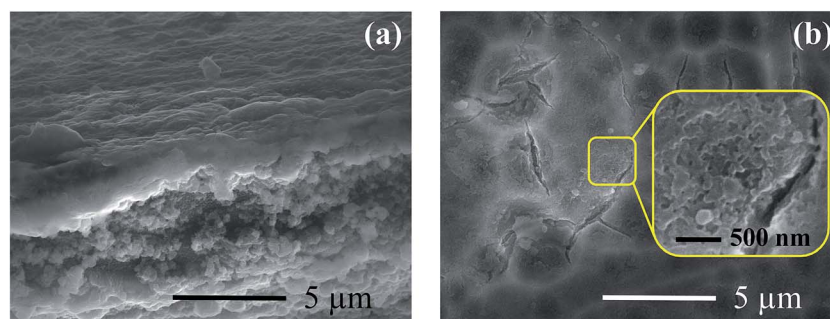


Fig. 10 SEM micrographs of the FeSiB amorphous ribbons after 7 reaction cycles, (a) side view; (b) top view.

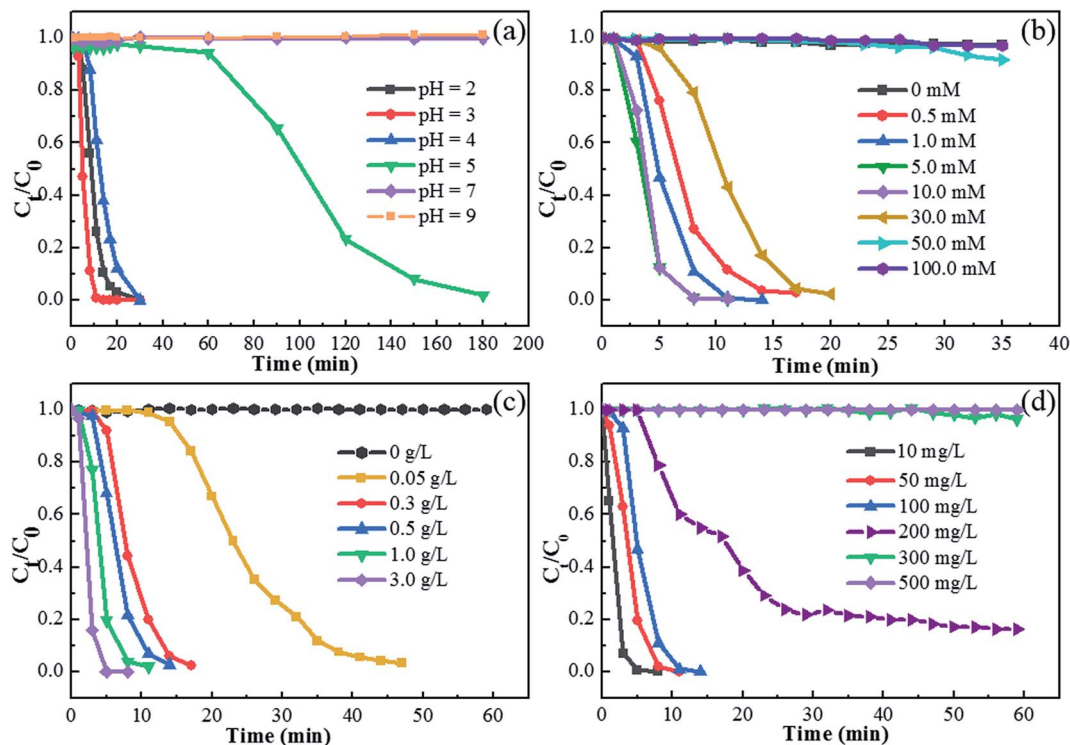
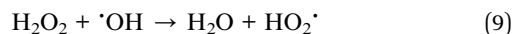


Fig. 11 Effects of (a) pH, (b)  $H_2O_2$  concentration, (c) ribbon dosage, and (d) dye concentration on the normalized concentration change of MB solutions during Fenton-like reactions using FePC amorphous ribbons.

investigated, as shown in Fig. 11(b). Various loads of  $H_2O_2$ , including 0 mM, 0.5 mM, 1 mM, 5 mM, 10 mM, 30 mM, 50 mM and 100 mM are added to MB solution, while other parameters are kept constant:  $T = 298$  K,  $pH = 3$ , ribbon dosage =  $0.5$  g  $L^{-1}$  and  $C_{MB} = 100$  mg  $L^{-1}$ . It is proved that  $H_2O_2$  is necessary for MB degradation at this reaction condition as no decolorization is observed even after 35 min without adding  $H_2O_2$ . With the concentration of  $H_2O_2$  increasing from 0.5 mM to 5 mM, the time required for complete degradation decreases from 14 min to 8 min. It also takes 8 min for the solution with 10 mM  $H_2O_2$  to finish decolorization. Then the degradation efficiency drops rapidly with further increasing of initial  $H_2O_2$  loads. When the initial concentration of  $H_2O_2$  is 30 mM, 95% MB is decolorized within 17 min, and no degradation of MB occurs within 30 min when the concentration of  $H_2O_2$  reaches 50 mM and 100 mM.

These results prove that appropriate addition of  $H_2O_2$  may accelerate the degradation process efficiently as presented in eqn (1)–(3). However, excessive  $H_2O_2$  is not conducive to the degradation process due to the well-known hydroxyl radical scavenging effect:<sup>45</sup>



The oxidation potential of the produced radicals  $HO_2 \cdot$  is much smaller than that of the hydroxyl radicals, making the oxidation of MB slower.

**Effect of ribbon dosage.** The effect of the FePC ribbon dosage on the MB degradation performance is investigated by adding different amounts of FePC ribbons into the reaction batches,

while keeping other reaction conditions constant:  $T = 298$  K,  $pH = 3$ ,  $C_{H_2O_2} = 1$  mM and  $C_{MB} = 100$  mg  $L^{-1}$ , as shown in Fig. 11(c). Without assistance from the FePC amorphous ribbon, no decomposition of MB is observed within an hour, implying the low degradation ability of  $H_2O_2$  itself. When the amount of ribbons increases from  $0.05$  g  $L^{-1}$  to  $0.3$  g  $L^{-1}$ ,  $0.5$  g  $L^{-1}$ ,  $1.0$  g  $L^{-1}$  and  $3$  g  $L^{-1}$ , the time required for 95% MB degradation drops from 44 min to 14 min, 11 min, 8 min and 5 min, continuously. Apparently, a larger dosage of amorphous ribbons leads to better degradation efficiency, due to the larger amount of available reaction sites.

**Effect of dye concentration.** The degradation efficiency at varied MB concentrations is presented in Fig. 11(d), while keeping other reaction conditions constant:  $T = 298$  K,  $pH = 3$ ,  $C_{H_2O_2} = 1$  mM and ribbon dosage =  $0.5$  g  $L^{-1}$ . A continuous decrease of the degradation efficiency with the increasing MB concentration is observed. It takes 5 min, 8 min and 11 min for the Fenton-like reaction to degrade  $10$  mg  $L^{-1}$ ,  $50$  mg  $L^{-1}$  and  $100$  mg  $L^{-1}$  MB solutions, respectively. When the initial MB concentration is  $200$  mg  $L^{-1}$ ,  $C_t/C_0$  decreases quickly to about 20% within 29 min, and then stays almost unchanged before 60 min. The decolorization of  $200$  mg  $L^{-1}$  MB is finished within 2 hours finally (data not shown). The fast degradation process in the first 29 min may have consumed most of the  $\cdot OH$  groups. After that,  $Fe^0$  from FePC ribbons acts as the reducing agent by losing 2 or 3 electrons to form  $Fe^{2+}$  or  $Fe^{3+}$ , while the large MB molecules get electrons and become smaller molecules.<sup>15</sup> This redox reaction is much slower than the Fenton-like reaction, explaining the low degradation efficiency after 29 min.

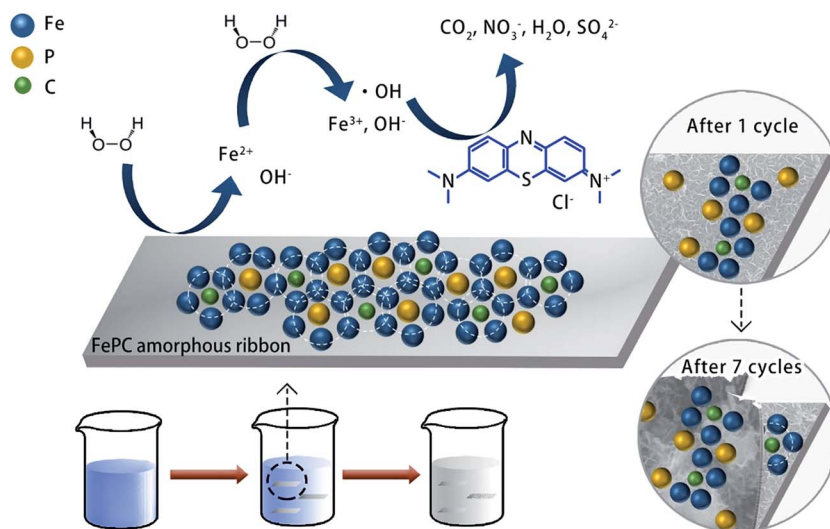


Fig. 12 Schematic diagrams of the pathway of MB degradation in Fenton-like reactions using FePC amorphous ribbons.

Only slight decolorization is visualized after 50 min when the MB concentration is  $300 \text{ mg L}^{-1}$ . When the MB concentration reaches  $500 \text{ mg L}^{-1}$ , no decomposition of MB occurs within 60 min. When the concentration of MB in the solution is too high (more than  $300 \text{ mg L}^{-1}$ ), the large MB molecules may cover the surface of FePC ribbons and impede  $\text{H}_2\text{O}_2$  to react with  $\text{Fe}^0$  to generate the powerful oxidizing  $\cdot\text{OH}$  groups. The FePC ribbon itself then starts to degrade MB as discussed before, but with a much lower efficiency. Thus the degradation performance of the solution decreases sharply when the initial MB concentration is high.

### Pathway of the degradation process

Based on the thorough analyses of the elemental information, surface morphology and electronic structure of FePC ribbons during MB degradation, as well as the cyclic tests, the pathway of this Fenton-like reaction can be drawn, as shown in Fig. 12. After adding FePC amorphous ribbons in the acidic MB solution with  $\text{H}_2\text{O}_2$ , the metallic iron, mostly from Fe–P clusters, react with  $\text{H}_2\text{O}_2$  and generate the strong oxidizing  $\cdot\text{OH}$  groups near the surface of the ribbons. The concentration difference and the mechanical stirring force drive the  $\cdot\text{OH}$  groups to spread into the solution to approach the MB molecules. Large MB molecules are then oxidized and decomposed into small molecules, including carbon dioxide, water, nitrate radicals and sulfate radicals. The continuous oxidation of iron from the FePC ribbon leaves the surface as 3D nanoporous structures, which then transform into cotton-like structures with increasing working time. The cotton-like structure mainly contains P, C and O elements, as well as a small amount of Fe element. Mechanical stirring drives the loose cotton-like layers to fall off from the ribbons gradually, which makes the underlying “fresh” FePC surface exposed to MB solution and prevents the drop of the degradation ability of FePC ribbons. This “self-renewing” characteristic extends the service life of FePC ribbons up to 19 cycles.

## Conclusions

In this work, we successfully found the higher dye degradation efficiency of FePC amorphous ribbons in Fenton-like reactions, compared to FeSiB amorphous ribbons. The galvanic cells formed due to the different strengths of Fe–P bonds and Fe–C bonds are believed to be the reason for the low reaction activation energy and the high degradation ability of FePC ribbons. Cyclic tests reveal that the extremely long service life of FePC ribbons comes from their “self-renewing” behaviour, as the used layers continually fall off from the main ribbons. The adaptability of this FePC amorphous ribbon which participated in the Fenton-like reaction is evaluated at varied pH values,  $\text{H}_2\text{O}_2$  concentration, ribbon dosage and dye concentration. The pathway of the reaction is sketched based on these thorough analyses. This work not only provides an efficient and low-cost solution for synthetic dye degradation, but also expands the application areas of FePC amorphous alloys.

## Conflicts of interest

There are no conflicts to declare.

## Acknowledgements

This work was supported by the National Natural Science Foundation of China (Grant No. 51501037, 51631003, 31570961, 51771054) and the Fundamental Research Funds for the Central Universities (Grant No. 2242016K41001).

## References

- 1 I. K. Konstantinou and T. A. Albanis, *Appl. Catal., B*, 2004, **49**, 1–14.
- 2 T. Robinson, G. McMullan, R. Marchant and P. Nigam, *Bioresour. Technol.*, 2001, **77**, 247–255.
- 3 *Advanced Nanomaterials for Water Engineering, Treatment, and Hydraulics*, ed. T. A. Saleh, IGI Global, Hershey, PA, USA, 2017.

- 4 V. K. Gupta, I. Ali, T. A. Saleh, A. Nayak and S. Agarwal, *RSC Adv.*, 2012, **2**, 6380–6388.
- 5 T. A. Saleh, I. B. Rachman and S. A. Ali, *Sci. Rep.*, 2017, **7**, 4573.
- 6 T. A. Saleh and V. K. Gupta, in *Nanomaterial and Polymer Membranes*, Elsevier, 2016.
- 7 G. Crini, *Bioresour. Technol.*, 2006, **97**, 1061–1085.
- 8 E. G. Garrido-Ramirez, B. K. G. Theng and M. L. Mora, *Appl. Clay Sci.*, 2010, **47**, 182–192.
- 9 I. M. Banat, P. Nigam, D. Singh and R. Marchant, *Bioresour. Technol.*, 1996, **58**, 217–227.
- 10 M. S. Lucas and J. A. Peres, *Dyes Pigm.*, 2006, **71**, 236–244.
- 11 A. D. Bokare, R. C. Chikate, C. V. Rode and K. M. Paknikar, *Environ. Sci. Technol.*, 2007, **41**, 7437–7443.
- 12 P. D. Mines, J. Byun, Y. Hwang, H. A. Patel, H. R. Andersen and C. T. Yavuz, *J. Mater. Chem. A*, 2016, **4**, 632–639.
- 13 C. A. Martinez-Huitle and E. Brillas, *Appl. Catal., B*, 2009, **87**, 105–145.
- 14 C. Q. Zhang, H. F. Zhang, M. Q. Lv and Z. Q. Hu, *J. Non-Cryst. Solids*, 2010, **356**, 1703–1706.
- 15 J. Q. Wang, Y. H. Liu, M. W. Chen, G. Q. Xie, D. V. Louzguine-Luzgin, A. Inoue and J. H. Perepezko, *Adv. Funct. Mater.*, 2012, **22**, 2567–2570.
- 16 J. F. Yang, X. F. Bian, Y. W. Bai, X. Q. Lv and P. Wang, *J. Non-Cryst. Solids*, 2012, **358**, 2571–2574.
- 17 P. Liu, J. L. Zhang, M. Q. Zha and C. H. Shek, *ACS Appl. Mater. Interfaces*, 2014, **6**, 5500–5505.
- 18 X. F. Wang, Y. Pan, Z. R. Zhu and J. L. Wu, *Chemosphere*, 2014, **117**, 638–643.
- 19 S. H. Xie, P. Huang, J. J. Kruzic, X. R. Zeng and H. X. Qian, *Sci. Rep.*, 2016, **6**, 21947.
- 20 S. Q. Chen, G. N. Yang, S. T. Luo, S. J. Yin, J. L. Jia, Z. Li, S. G. Gao, Y. Shao and K. F. Yao, *J. Mater. Chem. A*, 2017, **5**, 14230–14240.
- 21 Z. Jia, J. Kang, W. C. Zhang, W. M. Wang, C. Yang, H. Sun, D. Habibi and L. C. Zhang, *Appl. Catal., B*, 2017, **204**, 537–547.
- 22 Z. Deng, X. H. Zhang, K. C. Chan, L. Liu and T. Li, *Chemosphere*, 2017, **174**, 76–81.
- 23 C. Q. Zhang and Q. L. Sun, *J. Non-Cryst. Solids*, 2017, **470**, 93–98.
- 24 H. Y. Zhang, Y. P. Feng, Y. Y. Cheng, M. D. Baro, A. Altube, E. Garcia-Lecina, F. Alcaide, E. Pellicer, T. Zhang and J. Sort, *ACS Omega*, 2017, **2**, 653–662.
- 25 J. Q. Wang, Y. H. Liu, M. W. Chen, D. V. Louzguine-Luzgin, A. Inoue and J. H. Perepezko, *Sci. Rep.*, 2012, **2**, 418.
- 26 M. Iqbal and W. H. Wang, *IOP Conf. Ser.: Mater. Sci. Eng.*, 2014, **60**, UNSP 012035.
- 27 Y. F. Zhao, J. J. Si, J. G. Song, Q. Yang and X. D. Hui, *Mater. Sci. Eng., B*, 2014, **181**, 46–55.
- 28 M. Ramya, M. Karthika, R. Selvakumar, B. Raj and K. R. Ravi, *J. Alloys Compd.*, 2017, **696**, 185–192.
- 29 X. K. Luo, R. Li, J. Z. Zong, Y. Zhang, H. F. Li and T. Zhang, *Appl. Surf. Sci.*, 2014, **305**, 314–320.
- 30 Z. Deng, C. Zhang and L. Liu, *Intermetallics*, 2014, **52**, 9–14.
- 31 P. P. Wang, J. Q. Wang, H. Li, H. Yang, J. T. Huo, J. G. Wang, C. T. Chang, X. M. Wang, R. W. Li and G. Wang, *J. Alloys Compd.*, 2017, **701**, 759–767.
- 32 S. Das, S. Garrison and S. Mukherjee, *Adv. Eng. Mater.*, 2016, **18**, 214–218.
- 33 X. D. Qin, Z. W. Zhu, G. Liu, H. M. Fu, H. W. Zhang, A. M. Wang, H. Li and H. F. Zhang, *Sci. Rep.*, 2015, **5**, 18226.
- 34 Y. Y. Sha, I. Mathew, Q. Z. Cui, M. Clay, F. Gao, X. J. Zhang and Z. Y. Gu, *Chemosphere*, 2016, **144**, 1530–1535.
- 35 Y. Tang, Y. Shao, N. Chen, X. Liu, S. Q. Chen and K. F. Yao, *RSC Adv.*, 2015, **5**, 34032–34039.
- 36 J. F. Yang, X. F. Bian, M. L. Yuan, Y. W. Bai, Y. Liu, J. P. Fan, X. Q. Lu and K. K. Song, *J. Sol-Gel Sci. Technol.*, 2013, **67**, 362–367.
- 37 C. Q. Zhang, Z. W. Zhu, H. F. Zhang and Z. Q. Hu, *J. Non-Cryst. Solids*, 2012, **358**, 61–64.
- 38 Q. Li, J. F. Li, P. Gong, K. F. Yao, J. Gao and H. X. Li, *Intermetallics*, 2012, **26**, 62–65.
- 39 P. Duwez and S. C. H. Lin, *J. Appl. Phys.*, 1967, **38**, 4096–4097.
- 40 H. Wang, T. Hu and T. Zhang, *Phys. B*, 2013, **411**, 161–165.
- 41 X. H. Ma, X. H. Yang, Q. Li and S. F. Guo, *J. Alloys Compd.*, 2013, **577**, 345–350.
- 42 R. Xiang, S. X. Zhou, B. S. Dong, G. Q. Zhang, Z. Z. Li and Y. G. Wang, *J. Mater. Sci.: Mater. Electron.*, 2014, **25**, 2979–2984.
- 43 M. J. Shi, S. J. Pang and T. Zhang, *Intermetallics*, 2015, **61**, 16–20.
- 44 W. M. Yang, J. T. Huo, H. S. Liu, J. W. Li, L. J. Song, Q. Li, L. Xue, B. L. Shen and A. Inoue, *J. Alloys Compd.*, 2016, **684**, 29–33.
- 45 J. H. Ramirez, F. J. Maldonado-Hodar, A. F. Perez-Cadenas, C. Moreno-Castilla, C. A. Costa and L. M. Madeira, *Appl. Catal., B*, 2007, **75**, 312–323.
- 46 Y. F. Su, Z. Wu, Y. N. Wu, J. D. Yu, L. Sun and C. J. Lin, *J. Mater. Chem. A*, 2015, **3**, 8537–8544.
- 47 Z. Jia, W. C. Zhang, W. M. Wang, D. Habibi and L. C. Zhang, *Appl. Catal., B*, 2016, **192**, 46–56.
- 48 X. D. Qin, Z. K. Li, Z. W. Zhu, H. M. Fu, H. Li, A. M. Wang, H. W. Zhang and H. F. Zhang, *J. Mater. Sci. Technol.*, 2017, **33**, 1147–1152.
- 49 C. L. Qin, Q. F. Hu, Y. Y. Li, Z. F. Wang, W. M. Zhao, D. V. Louzguine-Luzgin and A. Inoue, *Mater. Sci. Eng., C*, 2016, **69**, 513–521.
- 50 F. Rueda, J. Mendialdua, A. Rodriguez, R. Casanova, Y. Barbaux, L. Gengembre and L. Jalowiecki, *J. Electron Spectrosc.*, 1996, **82**, 135–143.
- 51 P. H. Lo, W. T. Tsai, J. T. Lee and M. P. Hung, *J. Electrochem. Soc.*, 1995, **142**, 91–96.
- 52 C. J. Powell, *J. Electron Spectrosc.*, 2012, **185**, 1–3.
- 53 J. S. Hammond, J. W. Holubka, J. E. Devries and R. A. Dickie, *Corros. Sci.*, 1981, **21**, 239–253.
- 54 T. Fujiwara, *J. Phys. F: Met. Phys.*, 1982, **12**, 661–675.
- 55 S. X. Zhou, B. S. Dong, J. Y. Qin, D. R. Li, S. P. Pan, X. F. Bian and Z. B. Li, *J. Appl. Phys.*, 2012, **112**, 023514.
- 56 Y. Takahara and H. Matsuda, *Mater. Trans., JIM*, 1990, **31**, 835–841.
- 57 J. F. Wang, R. Li, N. B. Hua, L. Huang and T. Zhang, *Scr. Mater.*, 2011, **65**, 536–539.
- 58 H. R. Lashgari, Z. Chen, X. Z. Liao, D. Chu, M. Ferry and S. Li, *Mater. Sci. Eng., A*, 2015, **626**, 480–499.
- 59 X. F. Li, S. X. Liang, X. W. Xi, Z. Jia, S. K. Xie, H. C. Lin, J. P. Hu and L. C. Zhang, *Metals*, 2017, **7**, 273.
- 60 K. Hashimoto, *Appl. Surf. Sci.*, 2011, **257**, 8141–8150.
- 61 Z. H. Dan, A. Makino and N. Hara, *Mater. Trans.*, 2013, **54**, 1691–1696.